

Combining Quasiparticle Self-Consistent GW and Machine-Learned DFT+ U in Search of Half-Metallic Heuslers

Zefeng Cai,¹ Malcolm J. A. Jardine,¹ Maituo Yu,¹ Chenbo Min,¹ Jiatian Wu,¹
Hantian Liu,¹ Derek Dardzinski,¹ Christopher J. Palmström,^{2,3} and Noa Marom^{1,4,5,*}

¹*Department of Materials Science and Engineering,
Carnegie Mellon University, Pittsburgh, PA 15213, USA*

²*Materials Department, University of California-Santa Barbara, Santa Barbara, CA 93106, USA*

³*Department of Electrical and Computer Engineering,
University of California-Santa Barbara, Santa Barbara, CA 93106, USA*

⁴*Department of Chemistry, Carnegie Mellon University, Pittsburgh, PA 15213, USA*

⁵*Department of Physics, Carnegie Mellon University, Pittsburgh, PA 15213, USA*

(Dated: February 25, 2026)

Half-metallic Heusler compounds are of significant interest for spintronics. For device fabrication, compounds that can be epitaxially grown on III-V semiconductors are particularly attractive. We present a first-principles investigation of four Co-based and two Ni-based Heusler compounds that are lattice-matched to InAs. The results of density functional theory (DFT) using semi-local and hybrid functionals are compared to quasiparticle self-consistent GW (QPGW). We also consider DFT with machine-learned Hubbard U corrections [npj Computational Materials 6, 180 (2020)] with a new Bayesian optimization (BO) objective function to determine the U values that yield the closest agreement with the QPGW band structure and magnetic moments. We find that DFT+ U (BO) can adequately reproduce the key QPGW features in most cases. Our results reveal a strong method dependence of the degree of spin polarization at the Fermi level and, in some cases, even the dominant spin channel (majority or minority). Of the materials studied here, Co_2TiSn and Co_2ZrAl are the most likely to be half-metals, and Co_2MnIn is likely to be a near-half-metal.

I. INTRODUCTION

The Heuslers are a large family of ternary compounds with the formula X_2YZ , where X and Y are transition metals or rare earth elements and Z is a p -block element [1]. The sustained interest in Heuslers has been driven by their useful properties for a wide array of applications [2–8]. Magnetic Heusler compounds can serve as a ferromagnetic contact in magnetic tunnel junctions and magnetic spin valves [9, 10]. This can significantly improve the tunneling magnetoresistance (TMR) [11, 12], which is a key metric for efficient magnetic transport in a hard drive or a magnetic random access memory (MRAM) chip [13, 14]. Furthermore, the high spin polarization displayed by some Heuslers would make them ideal spin contacts to the semiconductor in spin-field effect transistors (FETs) [15], spin light emitting diodes [16], and spin-lasers [17]. More recently, some members of the Heusler family have been found to be topological insulators [18, 19]. Here, we focus on Heusler compounds that may exhibit half-metallicity [2, 20–23], meaning that one spin channel is metallic and the other is semiconducting. Half-metals are of interest for spintronics thanks to the promise of achieving close to 100% spin polarization at the Fermi level.

Chemically ordered films and atomically sharp, defect-free interfaces are desirable for spintronic devices because the preservation of half-metallicity in Heusler alloys and

spin-dependent transport across interfaces are highly sensitive to disorder, interfacial roughness, and impurities [13, 14, 24–36]. In particular, deviations from ideal L_{21} ordering in full-Heusler compounds have been shown to strongly suppress spin polarization [13] and increase magnetic damping [30]. Interfacial defects and disorder may introduce spin-flip scattering that reduces tunneling magnetoresistance and spin injection efficiency [31, 35, 36]. It has also been reported that half-metallicity may be degraded near surfaces and interfaces [37–43]. It has been found that the properties of the interface are governed by the local magnetic ordering and electronic structure of both the Heusler compound and the semiconductor [14, 44, 45].

These considerations motivate the search for Heuslers that can form epitaxial interfaces with appropriate substrates via growth techniques that enable precise stoichiometric and structural control. Ordered Heusler films can be fabricated by high temperature annealing when in contact with thermodynamically stable metals or insulating oxides [46, 47]. However, growing Heuslers on reactive semiconductors requires the use of molecular-beam epitaxy (MBE) [48] with individual elemental sources. Heusler compounds have been grown on various III-V semiconductors with a compatible FCC lattice. Thanks to the large compositional space of the Heusler family, which may be further expanded by substitutional alloying, it is possible to find lattice matched Heuslers for substrates with a wide range of lattice parameters including GaAs, InP, InAs, GaSb, and InSb [14, 49–51]. The growth of epitaxial Heusler/III-V interfaces is non-trivial because the elements comprising the Heusler (such

* Electronic mail: nmarom@andrew.cmu.edu

as Mn) may diffuse into and react with the III-V semiconductor at the interface [23, 52, 53], or conversely, elements from the semiconductor may out-diffuse into the Heusler film [54], requiring the use of barrier layers. Here, we focus on Heusler compounds predicted to have good lattice matching with InAs. InAs is attractive for spintronics and quantum computing applications due to its high electron mobility, large effective g -factor, strong spin-orbit coupling, and the absence of a Schottky barrier at the interface with various metals [55–58]. Because GaSb has a close lattice parameter to InAs, the materials considered here are also matched to GaSb. Considering the high cost of MBE, computer simulations can help select the most promising candidate materials for growth experiments.

There is a long history of first principles studies of Heuslers and related half-Heuslers starting from the seminal paper by de Groot *et al.*, which established the concept of half-metallicity in half-Heusler compounds [20]. Subsequent experimental work confirmed half-metallic behavior in materials such as NiMnSb [59–61]. This discovery motivated extensive computational investigations, predominantly using density functional theory (DFT) with local or semi-local exchange–correlation functionals [21, 62, 63]. In recent years, high-throughput computational screening has been employed to discover and design new Heusler candidates for diverse applications [64–73]. One limitation of such studies is that the predicted properties of Heusler compounds (and related classes of materials), including band gaps and magnetic properties, are highly sensitive to the choice of approximation for the exchange–correlation functional. Local and semi-local functionals may fail to reliably describe d -electron magnetism and half-metallicity in Heuslers and related materials [45, 74–80]. The deficiencies of (semi-)local DFT functionals may be attributed to a combination of the self-interaction error (SIE) and an inadequate treatment of strong correlation effects, both particularly pronounced for localized d - and f -electrons [81–84].

Hybrid functionals, in which a fraction of exact (Fock) exchange is mixed with semi-local exchange and correlation, often produce more accurate band gaps and band structures [85, 86]. However, hybrid functionals may overestimate exchange splitting and magnetic moments in transition-metals [87–91], which are the most common components in Heusler compounds, and may inaccurately describe spectral features near the Fermi level [92, 93]. Further improvement may be achieved by going beyond DFT. Many-body perturbation theory in the GW approximation [94], where G represents the Green’s function and W the screened Coulomb interaction, provides a more reliable description of correlated and magnetic materials [93, 95–98], including Heusler and half-Heusler compounds [23, 91, 99, 100]. In particular, the quasiparticle self-consistent GW (QP GW) method [101–103] eliminates the dependence on the mean-field starting point, which is a known limitation of one-shot G_0W_0 [104–108]. However, the high computational cost of hy-

brid functionals, and even more so of GW , limits the applicability of these methods to relatively small systems and precludes their utilization for studies of large interface models.

The DFT+ U method provides a balance between accuracy and efficiency by adding Hubbard U corrections that introduce an orbital-dependent on-site Coulomb interaction to (semi-)local functionals [109]. DFT+ U with an appropriate choice of the system-dependent U parameter(s) has been widely applied to correlated materials with localized d or f orbitals, such as transition-metal compounds [110–116]. For Heusler compounds and related materials, introducing Hubbard U corrections has been shown to improve the resulting electronic structure, including magnetic moments, spin polarization and band widths [38, 75, 117–124]. We have developed a method of machine learning the U values for a given material using Bayesian optimization (BO) with an objective function that aims to reproduce as closely as possible the band structure obtained from a higher-level reference method such as a hybrid functional or QP GW [125]. The DFT+ U (BO) method has enabled us to perform large-scale simulations of surfaces and interfaces [126–130], including Heusler/ III-V interfaces [45], which would not have been possible otherwise.

Here, we investigate the electronic and magnetic properties of four Co-based and two Ni-based Heusler compounds, whose lattice parameters are matched to InAs (or GaSb), as summarized in Table I. We compare the results obtained from QP GW to DFT with the generalized gradient approximation (GGA) of Perdew, Burke, and Ernzerhof (PBE) [131, 132] and the range-separated hybrid functional of Heyd-Scuseria-Ernzerhof (HSE) [133, 134], as well as PBE+ U (BO). For DFT+ U (BO), we have formulated a new objective function that includes the atomic magnetic moments in addition to the band structure, and we use QP GW as the reference method. The optimal U values obtained from the BO procedure enable PBE+ U (BO) to reproduce the key qualitative features of the QP GW electronic structure. We find that the choice of electronic structure method strongly influences the results. In some cases, different methods even provide *qualitatively* different predictions for whether a certain material is a half-metal and whether the spin polarization at the Fermi level is up or down. Of the materials studied here, only Co_2TiSn is unanimously predicted by all methods to be a half metal. Co_2ZrAl is predicted by all methods except HSE to be a half metal. Co_2MnIn is predicted by QP GW to be a near-half-metal with a high degree of minority spin polarization at the Fermi level. Our findings have significant implications for the reliability of high-throughput studies of magnetic Heuslers based on semi-local DFT.

TABLE I. Summary of the computed equilibrium lattice constant, total magnetic moment, spin polarization at the Fermi level, and effective U values applied to the d orbitals of the X and Y elements of each Heusler compound (a U correction was not applied to the Z element). The results of different electronic structure methods are compared for the total magnetic moment and the spin polarization at the Fermi level. A negative spin polarization indicates that the minority spin channel is dominant at the Fermi level.

| Material | a_0 (Å) | Total Magnetic Moment (μ_B) | | | | Spin Polarization (%) | | | | U (eV) | |
|----------------------|-----------|-----------------------------------|-------|-------|-------|-----------------------|--------|--------|--------|----------|-------|
| | | PBE | HSE | QPGW | PBE+U | PBE | HSE | QPGW | PBE+U | X | Y |
| Co ₂ MnIn | 5.980 | 4.455 | 7.374 | 6.448 | 5.853 | 85.98 | -64.36 | -94.62 | -94.29 | 2.252 | 0.751 |
| Co ₂ MnSn | 5.984 | 5.030 | 6.295 | 5.853 | 5.257 | 98.68 | -82.28 | -66.67 | 94.71 | 1.512 | 1.652 |
| Co ₂ TiSn | 6.082 | 1.997 | 2.009 | 1.996 | 1.997 | 100.00 | 100.00 | 100.00 | 99.98 | 3.534 | 3.654 |
| Co ₂ ZrAl | 6.063 | 0.999 | 1.304 | 1.000 | 0.999 | 100.00 | -32.83 | 100.00 | 100.00 | 1.331 | 9.379 |
| Ni ₂ MnSb | 6.059 | 4.044 | 4.462 | 4.662 | 4.620 | -30.77 | 14.94 | -43.03 | 7.85 | -1.512 | 5.155 |
| Ni ₂ MnSn | 6.056 | 4.108 | 4.613 | 4.780 | 4.466 | -67.52 | -65.63 | -69.93 | -56.95 | 2.392 | 2.352 |

II. METHODS

A. DFT+U(BO)

Previously, we had proposed Bayesian optimization as a practical approach for finding the optimal Hubbard U parameters for a given material within the Dudarev formulation of DFT+U [109]. The U corrections can be applied to any (semi-)local functional. Here, we use PBE. The BO objective function is formulated to reproduce as closely as possible the results of a reference method [125]. Originally, the objective function included the first two terms of Eq. 1, *i.e.*, the difference in the band gap, ΔGap (only used for semiconductors), and the difference in the band structure, ΔBand , weighted by α_1 and α_2 , respectively [125]. For magnetic materials, we now introduce a third term, ΔMag , representing the difference in atomic magnetic moments, with an additional weight α_3 :

$$f(\vec{U}) = -\alpha_1(\Delta\text{Gap})^2 - \alpha_2(\Delta\text{Band})^2 - \alpha_3(\Delta\text{Mag})^2 \quad (1)$$

where $\vec{U} = [U^1, U^2, \dots, U^n]$ represents the vector of U values applied to different elements and $U^i \in [-10, 10]$ eV. ΔGap is defined as:

$$\Delta\text{Gap} = E_g^{\text{ref}} - E_g^{\text{PBE+U}} \quad (2)$$

ΔBand is defined as an extension of the previous definition of the root mean squared difference between the PBE+U and the reference band structure [125, 135]:

$$\Delta\text{Band} = \sqrt{\frac{1}{N_E} \sum_{i=1}^{N_k} \sum_{j=1}^{N_b} w_i \left((\epsilon_{\text{ref}}^j[k_i] - \epsilon_{\text{ref},0}^j) - (\epsilon_{\text{PBE+U}}^j[k_i] - \epsilon_{\text{PBE+U},0}^j) \right)^2} \quad (3)$$

Here, N_E is the total number of eigenvalues included in the comparison, N_k is the number of k -points, and N_b is the number of bands selected for comparison. The weight factor w_i reflects the relative importance of each k -point based on its contribution to the Brillouin zone (BZ) volume. For k -paths with an equal number of k -points, it is normalized to ensure uniform sampling across the BZ:

$$\forall i \in I, \quad w_i = \frac{|\mathbf{k}_I|}{\sum_J |\mathbf{k}_J|}, \quad (4)$$

I and J are the index sets of k -points along the k -paths \mathbf{k}_I and \mathbf{k}_J , respectively. $|\mathbf{k}_I|$ denotes the length of the k -path \mathbf{k}_I in reciprocal space. Here, $\epsilon_{\text{ref},0}^j$ and $\epsilon_{\text{PBE+U},0}^j$ denote reference energy levels defined for band j in the reference method and in the PBE+U calculation, respectively. These reference energies are introduced to account for the fact that absolute energy levels are not directly comparable between calculations performed with different exchange-correlation functionals or pseudopotentials; only relative energy differences are physically meaningful. The reference level can be chosen by the user. common choices are the respective vacuum level or the valence band maximum (VBM) in both methods. For metallic systems, the reference energy is typically taken to be the Fermi level of each calculation. In the same vein, ΔMag is defined as the root mean squared error of the PBE+U magnetic moments compared to the reference method:

$$\Delta\text{Mag} = \sqrt{\frac{1}{N_i} \sum_{i=1}^{N_i} (m_{\text{ref}}^i - m_{\text{PBE+U}}^i)^2} \quad (5)$$

where N_i is the total number of atoms, and m is the magnetic moment produced by each method. Including the magnetic term leads to faster and more robust convergence of the BO algorithm, as shown in the SI.

Previously, we used HSE as the reference method [125]. However, as discussed above, for the materials studied

here, we consider QPGW as a more reliable choice. For metallic Heusler compounds, the objective function coefficients are set to $\alpha_1 = 0.0$, $\alpha_2 = 0.5$, and $\alpha_3 = 0.5$, assigning equal weights to the band structure and magnetic moments. N_b is set to 16 with 8 bands above and 8 bands below the Fermi level. The parameter κ , which controls the balance between exploration and exploitation in the BO upper confidence bound acquisition function [125], is set to 5. For the Heuslers studied here, Hubbard U corrections were applied to the d -orbitals of the transition-metal elements, X and Y, but not to the main-group element, Z. The BO algorithm was deemed converged if either (i) the difference in the objective function between two consecutive iterations was less than 0.0001 or (ii) the change in the interpolated optimum of the objective function over ten successive iterations was less than 0.005. The resulting U values for each material are summarized in Table I and BO convergence plots are provided in the SI.

B. Computational Details

All calculations were performed using the Vienna Ab initio Simulation Package (VASP) with the projector augmented wave (PAW) method [136–138]. All calculations used a plane-wave basis set with a kinetic energy cutoff of 400 eV and an energy convergence criterion of 10^{-6} eV. Spin-orbit coupling (SOC) was used for all calculations [139], including QPGW (an analysis of the effect of SOC on the electronic structure is provided in the SI). The recommended pseudopotentials provided by VASP (standard and *GW*) were used for all calculations. We included non-spherical contributions from the density gradient in the PAW spheres and applied a cutoff to the gradient field to restore the full lattice symmetry in order to account for magnetic anisotropy. The Brillouin zone was sampled using the Γ -centered scheme. For QPGW calculations, a $7 \times 7 \times 7$ k -point mesh was used. For PBE and HSE calculations a k -point mesh of $9 \times 9 \times 9$ was used.

Structural relaxation was performed with PBE using the conjugated gradients algorithm. The ionic relaxation was terminated when the change in total energy between two successive ionic steps fell below 10^{-5} eV. The resulting equilibrium lattice constants of all Heusler compounds studied here are listed in Table I.

The QPGW [103, 140] calculations were performed self-consistently with HSE used as the starting point. Based on convergence tests provided in the SI, seven self-consistent *GW* steps were performed. The total number of bands was set to 94 or 96, depending on the parallelization setup, corresponding to approximately twice the number of occupied bands for all six materials. The number of bands for which the self-energy shift was calculated was set to 78. The number of imaginary frequency and imaginary time grid points was set to 140. QPGW band structures were calculated via Wannier interpola-

tion using the `Wannier90` code [141].

The on-site magnetic moments were obtained by decomposing the Kohn-Sham orbitals onto the PAW projectors. The spin polarization percentage at the Fermi level was calculated as $\text{SP}\% = 100 P(E_f)$, where $P(E_f)$ is given by:

$$P(E_f) = \frac{\int_{E_f-\Delta}^{E_f+\Delta} [D_{\uparrow}(E) - D_{\downarrow}(E)] dE}{\int_{E_f-\Delta}^{E_f+\Delta} [D_{\uparrow}(E) + D_{\downarrow}(E)] dE} \quad (6)$$

Here, D_{\uparrow} and D_{\downarrow} are the spin-up (majority) and spin-down (minority) density of states (DOS). The integration is performed over an energy window of $2\Delta = 3.5 kT = 0.091$ eV centered at the Fermi level, chosen to match the full width at half maximum (FWHM) of the derivative of the Fermi-Dirac distribution at room temperature, thereby capturing the thermal broadening of the Fermi edge [142]. A sensitivity analysis of the SP value to the choice of integration window is provided in the SI. A negative sign of SP% indicates a minority spin polarization at the Fermi level. For the PBE, HSE, and PBE+U calculations, element- and orbital-decomposed band structures were obtained by projecting the Kohn-Sham states onto PAW on-site partial-wave projectors. Band structure and DOS plots were generated using the open-source package `vaspvis` [143], which is available on the Python Package Index (PyPI) via `pip install vaspvis`, and on GitHub at <https://github.com/caizefeng/vaspvis>. The DFT+U(BO) calculations were performed using the updated `BayesOpt4dftu` package, accessible at <https://github.com/caizefeng/BayesianOpt4dftu>.

III. RESULTS AND DISCUSSION

The Heusler alloys selected in this study are Co_2MnIn , Co_2MnSn , Co_2TiSn , Co_2ZrAl , Ni_2MnSb , and Ni_2MnSn . These compounds have a lattice mismatch below 1% with InAs or GaSb. Further screening criteria were applied to ensure that the compounds selected for this study possess a stable ferromagnetic ground state with the $Fm\bar{3}m$ symmetry at room temperature. It is worth noting that several other Co-, Ni-, or Ru-based full Heusler alloys also have nearly perfect lattice matching with InAs, but do not meet the magnetic stability criteria. For example, Co_2CrIn has a mismatch of only 0.02% with InAs but has been reported to exhibit a ferrimagnetic ground state [144]. Co_2NbSn , with a 0.89% mismatch to GaSb, has a low Curie temperature of 116 K and favors a competing $Pmma$ structure [145]. Ru_2MnAl , Ru_2MnGa , and Ru_2MnGe have excellent lattice matching to InAs, but prefer an antiferromagnetic state at room temperature [146].

Table I presents a summary of the total magnetic moments and the degree of spin polarization around the Fermi level obtained with different electronic structure methods. According to all methods considered here, the Ni-based compounds do not have a gap in either spin

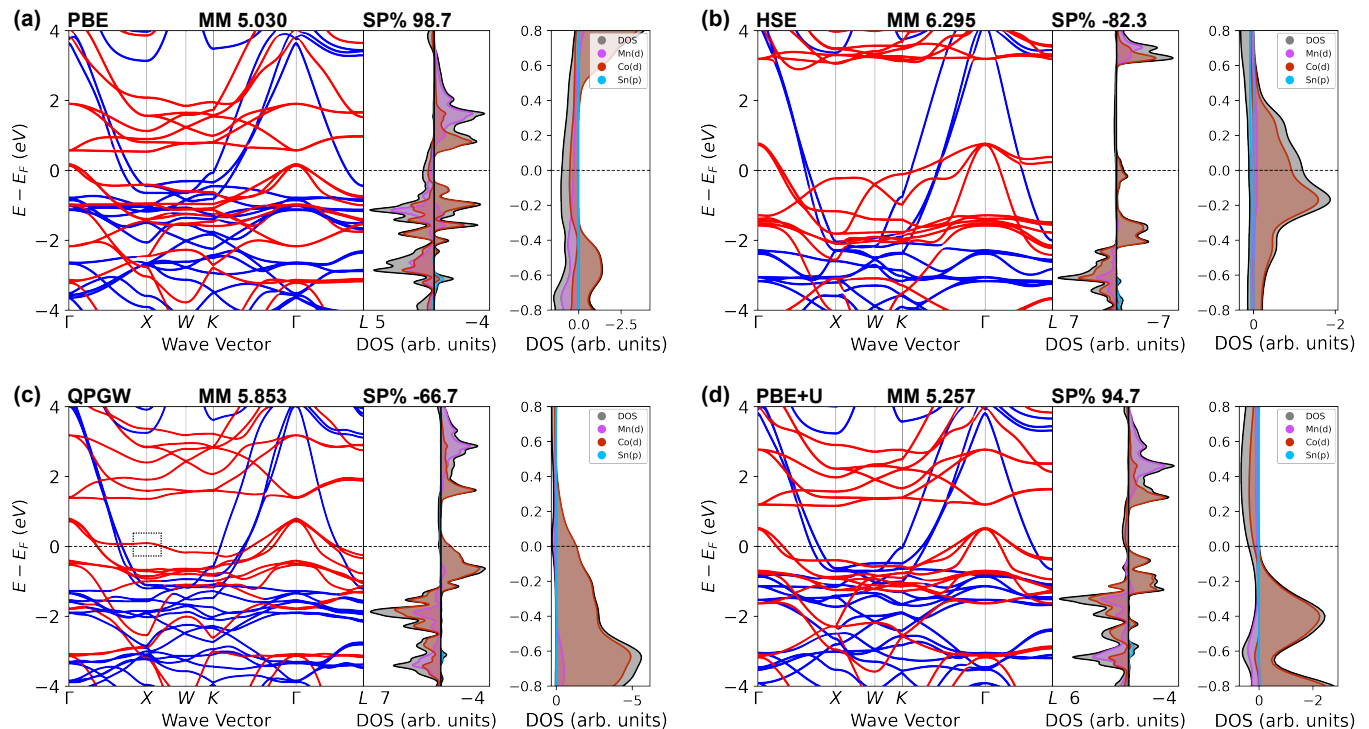


FIG. 1. Band structure and element-resolved DOS of Co_2MnSn calculated using (a) PBE, (b) HSE, (c) QPGW, and (d) PBE+U(BO). In the band-structure panels, the majority and minority spin channels are shown in blue and red, respectively. In the DOS panels, the majority and minority spin components are plotted on the left and right sides, respectively. The rightmost panels present a magnified view of the DOS around the Fermi level. The total magnetic moment (MM, in μ_B) and spin polarization percentage at the Fermi level (SP%) are listed for each method. Negative spin polarization indicates that the minority spin channel is dominant around the Fermi level. The dashed box in (c) highlights the flat minority-spin band near the Fermi level that gives rise to the minority-dominated spin polarization in the QPGW results.

channel and are not strongly spin-polarized around the Fermi level. Therefore, we focus the discussion in the main text on the Co-based compounds and provide the complete results for the Ni-based compounds in the SI. Co_2MnSn and Co_2MnIn exhibit relatively large magnetic moments due to the presence of the magnetic Mn atom in addition to Co. For these materials, the magnetic moments produced by different electronic structure methods vary significantly, with PBE giving the lowest value, HSE giving the highest value, and QPGW in between. For Co_2MnSn , experimental studies report total magnetic moments in the range of $5.05\text{--}5.12 \mu_B$ [123, 147, 148], which are closest to the PBE result of $5.03 \mu_B$ and the PBE+U(BO) value of $5.26 \mu_B$. Co_2TiSn and Co_2ZrAl have smaller magnetic moments because the Y-site element is non-magnetic. For these materials the results of different electronic structure methods are more consistent. For Co_2TiSn , all methods produce a total magnetic moment of $\sim 2 \mu_B$, in excellent agreement with experimental measurements [149–153]. For Co_2ZrAl , all methods (except HSE) predict a magnetic moment close to $1 \mu_B$, which is slightly higher than the experimentally measured value of approximately $0.7 \mu_B$ [154–156]. The measured magnetic moments of Ni_2MnSb range from 3.22 to $4.31 \mu_B$ [157, 158]. The scatter may be due to differences

in sample quality or stoichiometry. The computed values range from $4.04 \mu_B$ with PBE to $4.66 \mu_B$ with QPGW. Overall, both HSE and QPGW tend to overestimate the total magnetic moments relative to experiment for several compounds. Of the four Co-based compounds, only Co_2TiSn is unanimously predicted by all methods to be a half-metal. In the following, we present a detailed analysis of the origin of the differences between electronic structure methods.

Figure 1 shows the band structure and element-resolved DOS of Co_2MnSn obtained with PBE, HSE, QPGW, and PBE+U(BO). With the PBE functional, the DOS around the Fermi level is mainly contributed by the Co $3d$ and Mn $3d$ states. The DOS shows a half-metallic gap of 0.406 eV in the minority-spin channel (on the right-hand side of the DOS panels) and located 0.162 eV above the Fermi level. It should be noted that the position and width of the gap are determined from the band structure rather than from the DOS. Although the minority-spin gap appears sizable and may seem to intersect the Fermi level in the DOS plots of Figure 1(a), as well as in Figure 3(a) and Figure 5(a), a small but nonzero minority-spin density remains at the Fermi level, leading to a spin polarization below 100% (98.7% in this case). The apparent discrepancy arises because the band

structure is plotted along selected high-symmetry paths, which do not necessarily represent the full Brillouin-zone integration that determines the total DOS.

The HSE functional yields a considerably different band structure than PBE, as shown in panel b. The Mn d states are strongly exchange-split and shifted farther in energy above and below the Fermi level. The gap of 2.40 eV in the minority spin channel is considerably wider than with PBE and it is located 0.509 eV above the Fermi level. The DOS around the Fermi level is contributed predominantly by the Co $3d$ states, leading to minority spin polarization of -82.3%. The behavior of HSE likely originates from the overestimation of exchange splitting in d -electron systems by the non-local exchange term, which is a known limitation of this functional [88, 159].

With QPGW (panel c), the exchange splitting of the Mn d states is not as large as with HSE. The gap in the minority spin channel is 0.818 eV and it is located 4.756 eV above the Fermi level. The DOS around the Fermi level is dominated by the Co d states, similar to HSE, with a small contribution from the Mn d states. This results in a minority spin polarization of -66.7%. Although the QPGW band structure appears overall more similar to PBE than to HSE, a crucial difference is the rather flat minority band that lies slightly above the Fermi level around the X-point (indicated by the box in panel c). This is sufficient to flip the spin polarization around the Fermi level.

The results of PBE+U(BO) are in between PBE and QPGW, as shown in panel d. The gap in the minority spin channel is 0.905 eV, similar to QPGW. The DOS around the Fermi level is dominated by the Co d manifold. However, the flat minority band around the X-point lies below the Fermi level, leading to a majority spin polarization of 94.7%, similar to PBE. The interplay between the relative positions of the Co and Mn states d can thus lead to qualitatively different results with different electronic structure methods. A spin polarization of about 60% has been measured for Co_2MnSn by point-contact Andreev reflection (PCAR) [160]. We note that PCAR measures only the absolute value of the spin polarization irrespective of its sign [161, 162]. The absolute value of the spin polarization obtained from QPGW is close to the PCAR experiment, but we cannot determine whether the minority spin polarity is correct. This leaves us with the questions of whether Co_2MnSn is a half-metal, what is the dominant spin channel at the Fermi level, and which method should we trust?

To attempt to answer these questions, the orbital-resolved DOS of Co_2MnSn is compared with resonant photoemission spectroscopy (RPES) data [123] in Figure 2. The experimental data shown are difference spectra that were obtained therein by subtracting the off-resonance spectrum from the on-resonance spectrum to resolve the partial DOS of the Co- $3d$ and Mn- $3d$ states. The RPES data shows that the DOS close to the Fermi level is predominantly contributed by the Co- $3d$, whereas

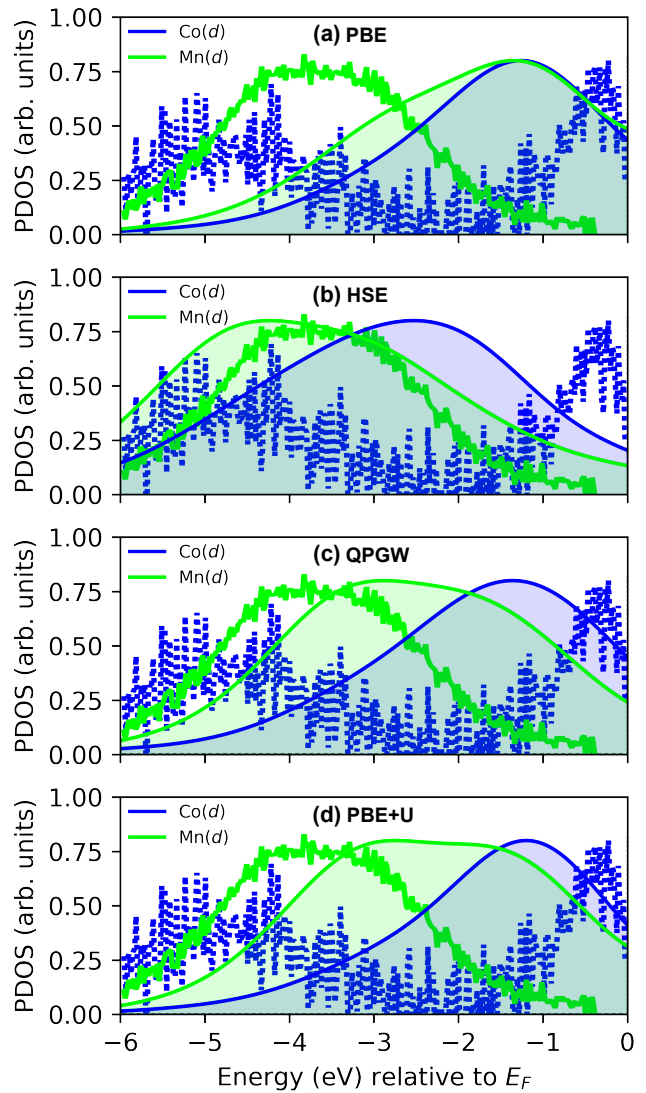


FIG. 2. Orbital-resolved DOS of Co_2MnSn calculated using (a) PBE, (b) HSE, (c) QPGW, and (d) PBE+U(BO), compared to the resonant photoemission spectroscopy (RPES) spectra of Co- $3d$ and Mn- $3d$, reproduced with permission from Ref. [123]. The computed spectra are broadened by a Gaussian with $\sigma = 0.77$ eV to simulate the resolution of the experiment. All spectra are normalized to the same maximum intensity. The satellite features between -6 eV and -2 eV in the experimental spectrum of Co- $3d$ are attributed in Ref. [123] to excitation effects that are not captured by the electronic structure methods used here.

the Mn- $3d$ states lie lower in energy, around -3.8 eV below the Fermi level. The satellite feature between -6 eV and -2 eV in the Co- $3d$ RPES spectrum was attributed in Ref. [123] to excited-state effects that are not captured by the electronic structure methods used here. We focus the comparison to experiment on the Co- $3d$ and Mn- $3d$ main peak positions. With PBE the Co- $3d$ and Mn- $3d$ overlap, which clearly contradicts the experimental data. HSE shifts the Mn- $3d$ peak to around -4 eV, which is close to the experiment, but the Co- $3d$ states are shifted too deep

to around -2.6 eV below the Fermi level, which deviates significantly from the experiment. With QPGW the Mn-3d peak is slightly too high and the Co-3d peak is slightly too low, providing the closest match to experiment of the methods considered here. The PBE+U(BO) partial DOS is very similar to QPGW. In Ref. [123] it was found that applying a Hubbard U correction of 3 eV to the Mn-3d states and no correction to the Co-3d provided the closest agreement with experiment. This is different than the U values of 1.512 eV for Co-3d and 1.652 eV for Mn-3d, which best reproduce the QPGW results. Detailed experimental characterization with spin-resolved angle-resolved photoemission spectroscopy (ARPES) [163, 164] would be needed to unambiguously determine which electronic structure method is the most reliable.

The case of Co_2MnIn , shown in Figure 3, is similar to Co_2MnSn in the sense that the interplay between the positions of the Co-3d and Mn-3d states leads to inconsistent results from different electronic structure methods. With PBE there is a very small gap of 0.103 eV in the minority-spin channel. The lower edge of this gap lies approximately 0.627 eV above the Fermi level. Similar to Co_2MnSn , there are contributions from both Co and Mn d states near the Fermi level, resulting in a spin polarization of 86.0%.

With HSE, the Mn d states are strongly exchange-split and pushed away from the Fermi level. The gap of 1.97 eV in the minority spin channel is much larger than with PBE and found 0.997 eV above the Fermi level. The main peaks of the Co d states are also pushed away from the Fermi level, leaving a relatively small minority spin density tail. The In p states contribute to the majority channel at the Fermi level, resulting in a minority spin polarization of -64.4%.

With QPGW the gap in the minority spin channel is 0.196 eV and it is located 1.199 eV above the Fermi level. The Mn d states are not near the Fermi level, although not as far away as with HSE. The DOS at the Fermi level is dominated by a large peak of minority spin Co d states, yielding a high spin polarization of -94.6%.

PBE+U(BO) produces a gap of 0.669 eV in the minority spin channel, which lies 0.499 eV above the Fermi level. The relative positions of the Co 3d and Mn 3d states is similar to QPGW with the DOS around the Fermi level dominated by a large Co 3d minority spin peak. Unlike pure PBE, which favors majority-spin polarization, PBE+U(BO) yields the same minority-spin polarization of -94.3% as QPGW. If we consider the results of QPGW to be the most reliable, then Co_2MnIn is expected to be a near-half-metal with a high spin polarization and a high density of states at the Fermi level, which would be advantageous for spintronic applications.

As mentioned above, Co_2TiSn , which has long been regarded as a prototypical example of a half-metallic Heusler compound [165–167], is the only material unanimously predicted by all methods used here to be a half-metal. As shown in Figure 4, there are still significant differences between the band structures produced by dif-

ferent methods with respect to the size of the gap in the minority spin channel and its position in energy and in k -space. PBE yields a gap of 0.605 eV, which is significantly smaller than the values of 1.291 eV, 1.563 eV, and 1.016 eV produced by HSE, QPGW, and PBE+U(BO), respectively. In addition, with PBE and QPGW the gap is located at the Γ -point, whereas with HSE and PBE+U(BO) it is located at the L-point. These differences in the band structure do not affect the outcome that only the majority spin Co d states contribute to the DOS at the Fermi level, which results in a 100% spin polarization. Experimentally, however, spin polarization values obtained via point-contact Andreev reflection (PCAR) are consistently lower, with reported values of $64\pm 2\%$, 57%, and $58.9\pm 2.2\%$ [150, 152, 168]. A possible explanation is that the spin polarization measured by PCAR is highly sensitive to perturbations such as defects, disorder, surface effects, or deviations from stoichiometry [169], even when the minority-spin gap edge is not located particularly close to the Fermi level.

Co_2ZrAl is predicted to be a half-metal by PBE, QPGW, and PBE+U(BO). With all three methods, only the majority spin Co d states contribute to the DOS at the Fermi level, leading to a 100% spin polarization, as shown in Figure 5. However, these three methods differ in the details of the band structure, particularly in the magnitude and location in k -space of the minority-spin gap. With PBE, the minority-spin gap is 0.515 eV, whereas QPGW predicts a substantially larger gap of 1.913 eV. The PBE+U(BO) result of 1.044 eV lies between these two values. In addition, with PBE and PBE+U(BO) the minority-spin gap is indirect between the X and Γ points, whereas with QPGW it is direct at the X-point. HSE produces a markedly different picture. The majority spin Co d states are pushed away from the Fermi level. As a result, the DOS at the Fermi level is dominated by minority-spin Co d states, with additional contributions from majority-spin Zr d states and only a marginal contribution of Al p states, leading to an overall minority spin polarization of -32.8%.

IV. CONCLUSION

In summary, we investigated the electronic structure and magnetic properties of six Heusler compounds in the cubic $L2_1$ ($Fm\bar{3}m$) phase with a stable ferromagnetic ground state that are lattice-matched to InAs and GaSb. We compared the results obtained using PBE, HSE, QPGW, and PBE+U(BO) with U values optimized to reproduce as closely as possible the QPGW band structure and magnetic moments. The results reveal a strong dependence of the magnitude and position of the gap in the minority spin channel, as well as the spin polarization at the Fermi level, on the electronic structure method used. In some cases, the predictions of different methods even differ qualitatively with respect to whether a material is expected to be a half-metal and the dom-

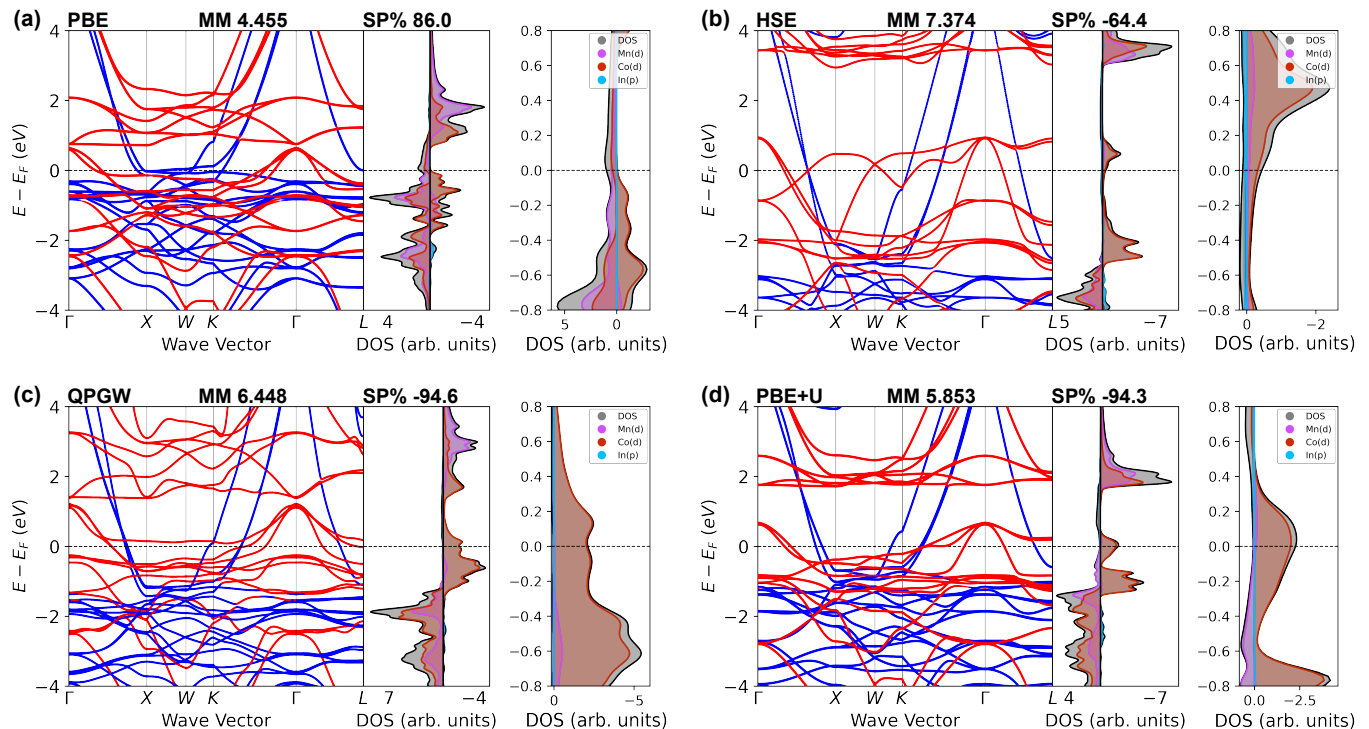


FIG. 3. Band structure and element-resolved DOS of Co_2MnIn calculated using (a) PBE, (b) HSE, (c) QPGW, and (d) PBE+U(BO). In the band-structure panels, the majority and minority spin channels are shown in blue and red, respectively. In the DOS panels, the majority and minority spin components are plotted on the left and right sides, respectively. The rightmost panels present a magnified view of the DOS around the Fermi level. The total magnetic moment (MM, in μ_B) and spin polarization percentage at the Fermi level (SP%) are listed for each method. Negative spin polarization indicates that the minority spin channel is dominant around the Fermi level.

inant spin channel (majority or minority) at the Fermi level. Our analysis shows that these differences arise from the treatment of d states with some systematic trends among methods. PBE tends to underestimate, whereas HSE tends to overestimate, the bandwidths and exchange splitting of the d manifolds, particularly in materials with strong d - d hybridization. The results of QPGW tend to be in the range between PBE and HSE. In most cases, PBE+U(BO) reproduces well the salient features of the QPGW band structure. The only exceptions found here are Co_2MnSn and Ni_2MnSb , for which the spin polarization at the Fermi level obtained with PBE+U(BO) differs qualitatively from QPGW. This may occur because the spin polarization at the Fermi level is not included in the BO objective function.

Of the materials considered here, we expect Co_2TiSn and Co_2ZrAl to be half-metals with a high degree of confidence, based on consistent predictions of all or most of the methods used here. In addition, if we consider the results of QPGW to be the most reliable, then Co_2MnIn is expected to be a near-half-metal with a high minority spin polarization at the Fermi level. It is also interesting to note that Co_2MnIn is predicted to have a high DOS at the Fermi level, in contrast to Co_2TiSn and Co_2ZrAl . A high DOS at the Fermi level could be an advantage for spintronic devices because more charge carriers would be

available to conduct current and because the spin polarization would be more robust to small perturbations.

Our findings have significant implications for the reliability of high-throughput studies of magnetic Heuslers and related materials based on semi-local DFT. We recommend further screening of candidate materials using more accurate methods prior to pursuing them experimentally. For simulations of interfaces and other large systems involving Heuslers, we suggest PBE+U(BO) as a practical solution for obtaining qualitatively correct results at a reasonable computational cost. However, we recommend verifying the results of PBE+U(BO) on a case by case basis and adapting the objective function if needed. This study also highlights the critical need for probing the band structure of Heuslers and related materials by ARPES, preferably spin resolved, in order to assess the accuracy and reliability of electronic structure methods for this important class of materials.

V. ACKNOWLEDGMENTS

We thank Paul Crowell from the University of Minnesota for helpful discussions. This research was funded by the Department of Energy through grant DE-SC0019274. This research used resources of the National

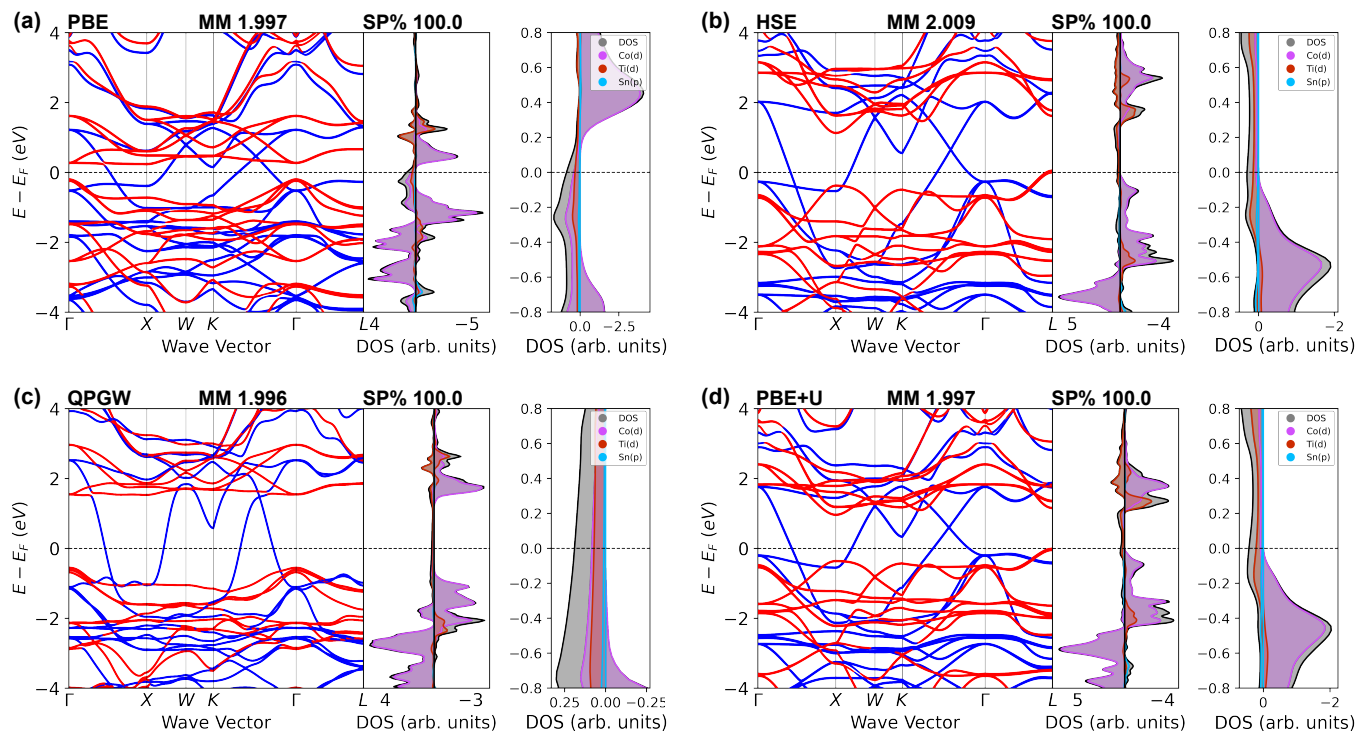


FIG. 4. Band structure and element-resolved DOS of Co_2TiSn calculated using (a) PBE, (b) HSE, (c) QPGW, and (d) PBE+U(BO). In the band-structure panels, the majority and minority spin channels are shown in blue and red, respectively. In the DOS panels, the majority and minority spin components are plotted on the left and right sides, respectively. The rightmost panels present a magnified view of the DOS around the Fermi level. The total magnetic moment (MM, in μ_B) and spin polarization percentage at the Fermi level (SP%) are listed for each method.

Energy Research Scientific Computing Center (NERSC), a DOE Office of Science User Facility supported by the Office of Science of the U.S. Department of Energy under contract no. DE-AC02-05CH11231.

VI. DATA AVAILABILITY

The VASP input and output files of the calculations presented here are available through Zenodo at zenodo.org/records/18705349 with DOI 10.5281/zenodo.18705349. The updated BayesOpt4dftu package is available at github.com/caizefeng/BayesianOpt4dftu. The vaspvis package is available on the Python Package Index (PyPI) via `pip install vaspvis`, and on GitHub at github.com/caizefeng/vaspvis.

- [1] A. A. Knowlton and O. C. Clifford, The Heusler alloys, *Trans. Faraday Soc.* **8**, 195 (1912).
- [2] C. Felser and A. Hirohata, *Heusler alloys* (Springer, 2015).
- [3] T. Graf, C. Felser, and S. S. Parkin, Simple rules for the understanding of Heusler compounds, *Progress in Solid State Chemistry* **39**, 1 (2011).
- [4] C. Felser, L. Wollmann, S. Chadov, G. H. Fecher, and S. S. Parkin, Basics and prospective of magnetic Heusler compounds, *APL Materials* **3**, 041518 (2015).
- [5] R. Farshchi and M. Ramsteiner, Spin injection from Heusler alloys into semiconductors: A materials perspective, *Journal of Applied Physics* **113**, 191101 (2013).
- [6] L. Wollmann, A. K. Nayak, S. S. Parkin, and C. Felser, Heusler 4.0: tunable materials, *Annual Review of Materials Research* **47**, 247 (2017).
- [7] T. Graf, S. S. Parkin, and C. Felser, Heusler compounds—a material class with exceptional properties, *IEEE Transactions on Magnetics* **47**, 367 (2010).
- [8] A. Hirohata and D. C. Lloyd, Heusler alloys for metal spintronics, *MRS Bulletin* **47**, 593 (2022).
- [9] T. Peterson, S. Patel, C. Geppert, K. Christie, A. Rath, D. Pennachio, M. Flatté, P. Voyles, C. Palmstrøm, and P. Crowell, Spin injection and detection up to room temperature in Heusler alloy/n-GaAs spin valves, *Physical*

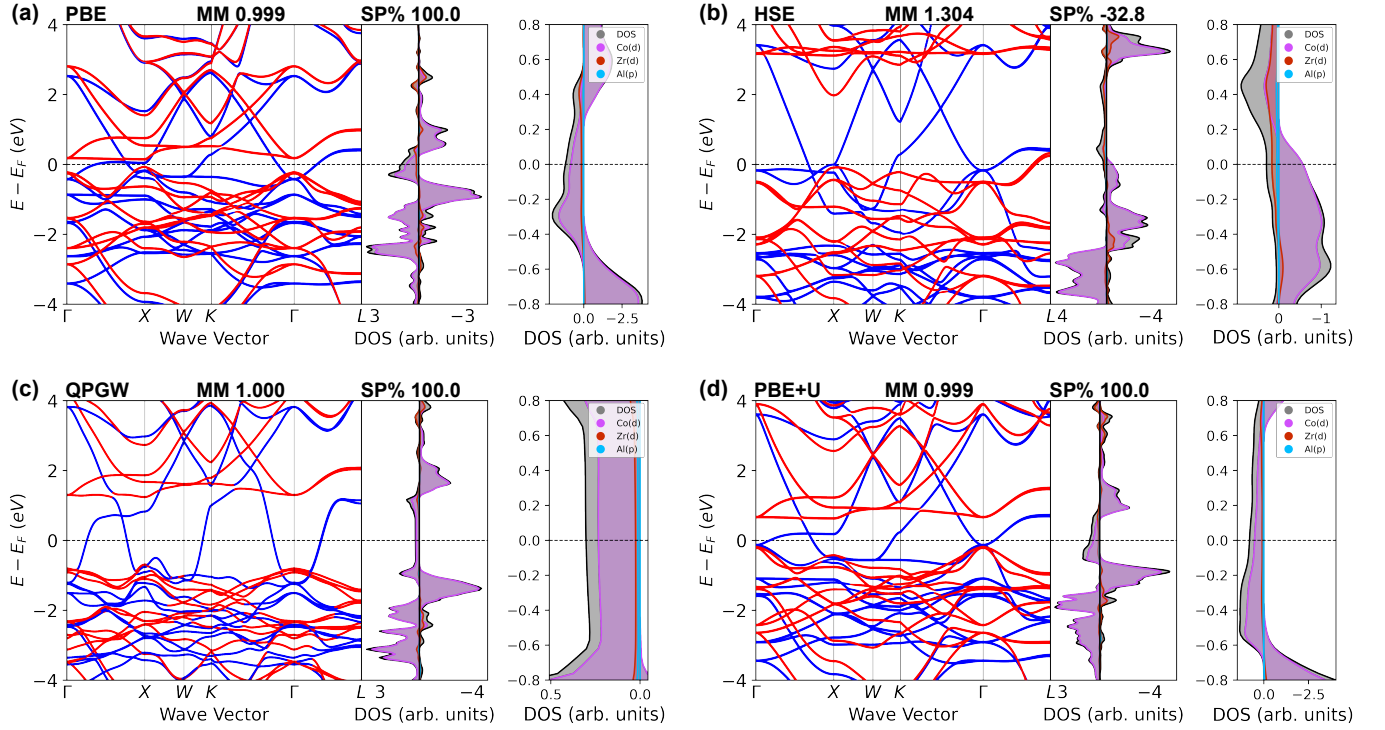


FIG. 5. Band structure and element-resolved DOS of Co_2ZrAl calculated using (a) PBE, (b) HSE, (c) QPGW, and (d) PBE+U(BO). In the band-structure panels, the majority and minority spin channels are shown in blue and red, respectively. In the DOS panels, the majority and minority spin components are plotted on the left and right sides, respectively. The rightmost panels present a magnified view of the DOS around the Fermi level. The total magnetic moment (MM, in μ_B) and spin polarization percentage at the Fermi level (SP%) are listed for each method. Negative spin polarization indicates that the minority spin channel is dominant around the Fermi level.

- Review B **94**, 235309 (2016).
- [10] R. Sahoo, L. Wollmann, S. Selle, T. Höche, B. Ernst, A. Kalache, C. Shekhar, N. Kumar, S. Chadov, C. Felser, *et al.*, Compensated ferrimagnetic tetragonal Heusler thin films for antiferromagnetic spintronics, *Advanced Materials* **28**, 8499 (2016).
- [11] S. Kämmerer, A. Thomas, A. Hütten, and G. Reiss, Co_2MnSi Heusler alloy as magnetic electrodes in magnetic tunnel junctions, *Applied Physics Letters* **85**, 79 (2004).
- [12] S. Okamura, A. Miyazaki, S. Sugimoto, N. Tezuka, and K. Inomata, Large tunnel magnetoresistance at room temperature with a Co_2FeAl full-Heusler alloy electrode, *Applied Physics Letters* **86**, 232503 (2005).
- [13] K. Elphick, W. Frost, M. Samiepour, T. Kubota, K. Takanashi, H. Sukegawa, S. Mitani, and A. Hirohata, Heusler alloys for spintronic devices: review on recent development and future perspectives, *Science and Technology of Advanced Materials* **22**, 235 (2021).
- [14] C. J. Palmstrøm, Heusler compounds and spintronics, *Progress in Crystal Growth and Characterization of Materials* **62**, 371 (2016).
- [15] S. Datta and B. Das, Electronic analog of the electro-optic modulator, *Applied Physics Letters* **56**, 665 (1990).
- [16] M. Holub, J. Shin, D. Saha, and P. Bhattacharya, Electrical spin injection and threshold reduction in a semiconductor laser, *Physical Review Letters* **98**, 146603 (2007).
- [17] P. Bhattacharya, D. Basu, A. Das, and D. Saha, Quantum dot polarized light sources, *Semiconductor Science and Technology* **26**, 014002 (2010).
- [18] B. Yan and C. Felser, Topological materials: Weyl semimetals, *Annual Review of Condensed Matter Physics* **8**, 337 (2017).
- [19] S. Chadov, X. Qi, J. Kübler, G. H. Fecher, C. Felser, and S. C. Zhang, Tunable multifunctional topological insulators in ternary Heusler compounds, *Nature Materials* **9**, 541 (2010).
- [20] R. De Groot, F. Mueller, P. Van Engen, and K. Buschow, New class of materials: half-metallic ferromagnets, *Physical Review Letters* **50**, 2024 (1983).
- [21] S. Ishida, S. Fujii, S. Kashiwagi, and S. Asano, Search for half-metallic compounds in Co_2MnZ ($Z = \text{IIIb, IVb, Vb}$ element), *Journal of the Physical Society of Japan* **64**, 2152 (1995).
- [22] I. Galanakis, K. Özdoğan, E. Şaşıoğlu, and B. Aktaş, Ferrimagnetism and antiferromagnetism in half-metallic Heusler alloys, *Physica Status Solidi (a)* **205**, 1036 (2008).
- [23] S. Nishihaya, M. J. A. Jardine, H. S. Inbar, A. Goswami, J. T. Dong, A. N. Engel, Y.-H. Chang, C. P. Dempsey, M. Hashimoto, D. Lu, N. Marom, and C. J. Palmstrøm, Near-half-metallic state in the half-Heusler PtMnSb film on a III-V substrate, *Phys. Rev. Mater.* **9**, 044403 (2025).

- [24] D. Orgassa, H. Fujiwara, T. Schulthess, and W. Butler, First-principles calculation of the effect of atomic disorder on the electronic structure of the half-metallic ferromagnet NiMnSb, *Physical Review B* **60**, 13237 (1999).
- [25] W. Van Roy, J. De Boeck, B. Brijs, and G. Borghs, Epitaxial NiMnSb films on GaAs (001), *Applied Physics Letters* **77**, 4190 (2000).
- [26] Y. Sakuraba, J. Nakata, M. Oogane, H. Kubota, Y. Ando, A. Sakuma, and T. Miyazaki, Fabrication of Co₂MnAl Heusler alloy epitaxial film using Cr buffer layer, *Japanese Journal of Applied Physics* **44**, 6535 (2005).
- [27] C. Adelman, J. Xie, C. Palmstrøm, J. Strand, X. Lou, J. Wang, and P. Crowell, Effects of doping profile and post-growth annealing on spin injection from Fe into (Al,Ga)As heterostructures, *Journal of Vacuum Science & Technology B: Microelectronics and Nanometer Structures Processing, Measurement, and Phenomena* **23**, 1747 (2005).
- [28] T. Marukame, T. Ishikawa, S. Hakamata, K.-i. Matsuda, T. Uemura, and M. Yamamoto, Highly spin-polarized tunneling in fully epitaxial Co₂Cr_{0.6}Fe_{0.4}Al/MgO/Co₅₀Fe₅₀ magnetic tunnel junctions with exchange biasing, *Applied Physics Letters* **90** (2007).
- [29] B. Schultz, N. Marom, D. Naveh, X. Lou, C. Adelman, J. Strand, P. Crowell, L. Kronik, and C. Palmstrøm, Spin injection across the Fe/GaAs interface: Role of interfacial ordering, *Physical Review B* **80**, 201309 (2009).
- [30] C. Guillemard, S. Petit-Watelot, T. Devolder, L. Pasquier, P. Boulet, S. Migot, J. Ghanbaja, F. Bertran, and S. Andrieu, Issues in growing Heusler compounds in thin films for spintronic applications, *Journal of Applied Physics* **128** (2020).
- [31] J. De Boeck, W. Van Roy, V. Motsnyi, Z. Liu, K. Dessein, and G. Borghs, Hybrid epitaxial structures for spintronics, *Thin Solid Films* **412**, 3 (2002).
- [32] S. S. Parkin, C. Kaiser, A. Panchula, P. M. Rice, B. Hughes, M. Samant, and S.-H. Yang, Giant tunnelling magnetoresistance at room temperature with MgO (100) tunnel barriers, *Nature Materials* **3**, 862 (2004).
- [33] S. Yuasa, T. Nagahama, A. Fukushima, Y. Suzuki, and K. Ando, Giant room-temperature magnetoresistance in single-crystal Fe/MgO/Fe magnetic tunnel junctions, *Nature Materials* **3**, 868 (2004).
- [34] J. P. Velev, P. A. Dowben, E. Y. Tsybmal, S. J. Jenkins, and A. Caruso, Interface effects in spin-polarized metal/insulator layered structures, *Surface Science Reports* **63**, 400 (2008).
- [35] C. Wang, A. Kohn, S. Wang, L. Chang, S.-Y. Choi, A. Kirkland, A. Petford-Long, and R. Ward, Structural characterization of interfaces in epitaxial Fe/MgO/Fe magnetic tunnel junctions by transmission electron microscopy, *Physical Review B* **82**, 024428 (2010).
- [36] A. Hirohata, K. Elphick, D. C. Lloyd, and S. Mizukami, Interfacial quality to control tunnelling magnetoresistance, *Frontiers in Physics* **10**, 1007989 (2022).
- [37] S. Picozzi, A. Continenza, and A. J. Freeman, Spin injection at Heusler/semiconductor interfaces: First-principles determination of potential discontinuity and half-metallicity, *Journal of Applied Physics* **94**, 4723 (2003).
- [38] S. Khosravizadeh, S. J. Hashemifar, and H. Akbarzadeh, First-principles study of the Co₂FeSi (001) surface and Co₂FeSi/GaAs (001) interface, *Physical Review B* **79**, 235203 (2009).
- [39] I. Galanakis and P. Mavropoulos, Spin-polarization and electronic properties of half-metallic Heusler alloys calculated from first principles, *Journal of Physics: Condensed Matter* **19**, 315213 (2007).
- [40] I. Galanakis, M. Ležaić, G. Bihlmayer, and S. Blügel, Interface properties of NiMnSb/InP and NiMnSb/GaAs contacts, *Physical Review B—Condensed Matter and Materials Physics* **71**, 214431 (2005).
- [41] I. Galanakis, Surface properties of the half-and full-Heusler alloys, *Journal of Physics: Condensed Matter* **14**, 6329 (2002).
- [42] S. J. Jenkins, Ternary half-metallics and related binary compounds: Stoichiometry, surface states, and spin, *Phys. Rev. B* **70**, 245401 (2004).
- [43] S. Jenkins and D. King, Formation of interface states on a half-metal surface, *Surface Science* **501**, L185 (2002).
- [44] A. Rath, C. Sivakumar, C. Sun, S. J. Patel, J. S. Jeong, J. Feng, G. Stecklein, P. A. Crowell, C. J. Palmstrøm, W. H. Butler, and P. M. Voyles, Reduced interface spin polarization by antiferromagnetically coupled Mn segregated to the Co₂MnSi/GaAs (001) interface, *Phys. Rev. B* **97**, 045304 (2018).
- [45] B. Heischmidt, M. Yu, D. Dardzinski, J. Etheridge, S. Moayedpour, V. S. Pribiag, P. A. Crowell, and N. Marom, First principles study of the electronic structure of the Ni₂MnIn/InAs and Ti₂MnIn/InSb interfaces, *Phys. Rev. Mater.* **7**, 026203 (2023).
- [46] Y. Sakuraba, J. Nakata, M. Oogane, H. Kubota, Y. Ando, A. Sakuma, and T. Miyazaki, Huge spin-polarization of L₂₁-ordered Co₂MnSi epitaxial Heusler alloy film, *Japanese Journal of Applied Physics* **44**, L1100 (2005).
- [47] N. Tezuka, N. Ikeda, A. Miyazaki, S. Sugimoto, M. Kikuchi, and K. Inomata, Tunnel magnetoresistance for junctions with epitaxial full-Heusler Co₂FeAl_{0.5}Si_{0.5} electrodes with B2 and L₂₁ structures, *Applied Physics Letters* **89**, 112514 (2006).
- [48] A. Hirohata, M. Kikuchi, N. Tezuka, K. Inomata, J. Claydon, Y. Xu, and G. Van der Laan, Heusler alloy/semiconductor hybrid structures, *Current Opinion in Solid State and Materials Science* **10**, 93 (2006).
- [49] V. Alijani, S. Ouardi, G. H. Fecher, J. Winterlik, S. S. Naghavi, X. Kozina, G. Stryganyuk, C. Felser, E. Ikenaga, Y. Yamashita, S. Ueda, and K. Kobayashi, Electronic, structural, and magnetic properties of the half-metallic ferromagnetic quaternary Heusler compounds CoFeMnZ (Z = Al, Ga, Si, Ge), *Phys. Rev. B* **84**, 224416 (2011).
- [50] G. Gao, L. Hu, K. Yao, B. Luo, and N. Liu, Large half-metallic gaps in the quaternary Heusler alloys CoFeCrZ (Z=Al, Si, Ga, Ge): A first-principles study, *Journal of Alloys and Compounds* **551**, 539 (2013).
- [51] E. Valerio, C. Grigorescu, S. Manea, F. Guinneton, W. Branford, and M. Autric, Pulsed laser deposition of thin films of various full Heusler alloys Co₂MnX (X=Si, Ga, Ge, Sn, SbSn) at moderate temperature, *Applied Surface Science* **247**, 151 (2005).
- [52] K. M. Law, A. S. Thind, M. Pendharkar, S. J. Patel, J. J. Phillips, C. J. Palmstrom, J. Gazquez, A. Borisevich, R. Mishra, and A. J. Hauser, Formation of Mn-rich interfacial phases in Co₂Fe_xMn_{1-x}Si thin films, *Journal of Magnetism and Magnetic Materials* **593**, 171884

- (2024).
- [53] L. Singh, Z. Barber, A. Kohn, A. Petford-Long, Y. Miyoshi, Y. Bugoslavsky, and L. Cohen, Interface effects in highly oriented films of the Heusler alloy Co_2MnSi on GaAs (001), *Journal of Applied Physics* **99** (2006).
- [54] K. Hamaya and M. Yamada, Semiconductor spintronics with Co_2 -Heusler compounds, *MRS Bulletin* **47**, 584 (2022).
- [55] T. Zhang, T. Lindemann, G. C. Gardner, S. Gronin, T. Wu, and M. J. Manfra, Mobility exceeding $100000 \text{ cm}^2/\text{v s}$ in modulation-doped shallow InAs quantum wells coupled to epitaxial aluminum, *Physical Review Materials* **7**, 056201 (2023).
- [56] S. Prabhakar, J. E. Reynolds, and R. Melnik, Manipulation of the Landé g factor in InAs quantum dots through the application of anisotropic gate potentials: Exact diagonalization, numerical, and perturbation methods, *Physical Review B* **84**, 155208 (2011).
- [57] K. Takase, Y. Ashikawa, G. Zhang, K. Tateno, and S. Sasaki, Highly gate-tuneable Rashba spin-orbit interaction in a gate-all-around InAs nanowire metal-oxide-semiconductor field-effect transistor, *Scientific Reports* **7**, 930 (2017).
- [58] B. Feng, S. Huang, J. Wang, D. Pan, J. Zhao, and H. Xu, Schottky barrier heights at the interfaces between pure-phase InAs nanowires and metal contacts, *Journal of Applied Physics* **119** (2016).
- [59] K. E. H. M. Hanssen, P. E. Mijnders, L. P. L. M. Rabou, and K. H. J. Buschow, Positron-annihilation study of the half-metallic ferromagnet NiMnSb: Experiment, *Phys. Rev. B* **42**, 1533 (1990).
- [60] K. E. H. M. Hanssen and P. E. Mijnders, Positron-annihilation study of the half-metallic ferromagnet NiMnSb: Theory, *Phys. Rev. B* **34**, 5009 (1986).
- [61] M. M. Kirillova, A. A. Makhnev, E. I. Shreder, V. P. Dyakina, and N. B. Gorina, Interband optical absorption and plasma effects in half-metallic XMnY ferromagnets, *Physica Status Solidi (b)* **187**, 231 (1995).
- [62] I. Galanakis, P. H. Dederichs, and N. Papanikolaou, Origin and properties of the gap in the half-ferromagnetic Heusler alloys, *Phys. Rev. B* **66**, 134428 (2002).
- [63] I. Galanakis, P. Dederichs, and N. Papanikolaou, Slater-Pauling behavior and origin of the half-metallicity of the full-Heusler alloys, *Physical Review B* **66**, 174429 (2002).
- [64] A. Roy, J. W. Bennett, K. M. Rabe, and D. Vanderbilt, Half-Heusler semiconductors as piezoelectrics, *Phys. Rev. Lett.* **109**, 037602 (2012).
- [65] B. Yan and A. de Visser, Half-Heusler topological insulators, *MRS Bulletin* **39**, 859 (2014).
- [66] S. Sanvito, C. Oses, J. Xue, A. Tiwari, M. Zic, T. Archer, P. Tozcan, M. Venkatesan, M. Coey, and S. Curtarolo, Accelerated discovery of new magnets in the Heusler alloy family, *Science Advances* **3**, e1602241 (2017).
- [67] W. Rotjanapittayakul, J. Prasongkit, I. Rungger, S. Sanvito, W. Pijitrojana, and T. Archer, Search for alternative magnetic tunnel junctions based on all-Heusler stacks, *Physical Review B* **98**, 054425 (2018).
- [68] J. Ma, V. I. Hegde, K. Munira, Y. Xie, S. Keshavarz, D. T. Mildebrath, C. Wolverton, A. W. Ghosh, and W. Butler, Computational investigation of half-Heusler compounds for spintronics applications, *Physical Review B* **95**, 024411 (2017).
- [69] J. Ma, J. He, D. Mazumdar, K. Munira, S. Keshavarz, T. Lovorn, C. Wolverton, A. W. Ghosh, and W. H. Butler, Computational investigation of inverse Heusler compounds for spintronics applications, *Physical Review B* **98**, 094410 (2018).
- [70] S. Jiang and K. Yang, Review of high-throughput computational design of Heusler alloys, *Journal of Alloys and Compounds* **867**, 158854 (2021).
- [71] S. Jiang, S. Nazir, and K. Yang, High-throughput design of interfacial perpendicular magnetic anisotropy at Heusler/MgO heterostructures, *ACS Applied Materials & Interfaces* **14**, 9734 (2022).
- [72] S. Jiang and K. Yang, High-throughput design of perpendicular magnetic anisotropy at quaternary Heusler and MgO interfaces, *npj Computational Materials* **9**, 123 (2023).
- [73] R. Hilgers, D. Wortmann, and S. Blügel, Machine learning-based estimation and explainable artificial intelligence-supported interpretation of the critical temperature from magnetic ab initio Heusler alloys data, *Phys. Rev. Mater.* **9**, 044412 (2025).
- [74] K. Nawa and Y. Miura, Exploring half-metallic Co-based full Heusler alloys using a DFT+U method combined with linear response approach, *RSC Adv.* **9**, 30462 (2019).
- [75] H. C. Kandpal, G. H. Fecher, C. Felser, and G. Schönhense, Correlation in the transition-metal-based Heusler compounds Co_2MnSi and Co_2FeSi , *Physical Review B* **73**, 094422 (2006).
- [76] S. V. Faleev, Y. Ferrante, J. Jeong, M. G. Samant, B. Jones, and S. S. Parkin, Unified explanation of chemical ordering, the Slater-Pauling rule, and half-metallicity in full Heusler compounds, *Physical Review B* **95**, 045140 (2017).
- [77] S. V. Faleev, Y. Ferrante, J. Jeong, M. G. Samant, B. Jones, and S. S. Parkin, Origin of the tetragonal ground state of Heusler compounds, *Physical Review Applied* **7**, 034022 (2017).
- [78] S. V. Faleev, Y. Ferrante, J. Jeong, M. G. Samant, B. Jones, and S. S. P. Parkin, Heusler compounds with perpendicular magnetic anisotropy and large tunneling magnetoresistance, *Phys. Rev. Mater.* **1**, 024402 (2017).
- [79] V. I. Anisimov, F. Aryasetiawan, and A. I. Lichtenstein, First-principles calculations of the electronic structure and spectra of strongly correlated systems: the LDA+U method, *Journal of Physics: Condensed Matter* **9**, 767 (1997).
- [80] S. Kobayashi, Y. Nohara, S. Yamamoto, and T. Fujiwara, GW approximation with LSDA + U method and applications to NiO, MnO, and V_2O_3 , *Phys. Rev. B* **78**, 155112 (2008).
- [81] J. P. Perdew and A. Zunger, Self-interaction correction to density-functional approximations for many-electron systems, *Phys. Rev. B* **23**, 5048 (1981).
- [82] P. Mori-Sánchez, A. J. Cohen, and W. Yang, Localization and delocalization errors in density functional theory and implications for band-gap prediction, *Physical Review Letters* **100**, 146401 (2008).
- [83] A. J. Cohen, P. Mori-Sánchez, and W. Yang, Insights into current limitations of density functional theory, *Science* **321**, 792 (2008).
- [84] G. Kotliar, S. Y. Savrasov, K. Haule, V. S. Oudovenko, O. Parcollet, and C. Marianetti, Electronic structure

- calculations with dynamical mean-field theory, *Reviews of Modern Physics* **78**, 865 (2006).
- [85] F. Shi, M. Si, J. Xie, K. Mi, C. Xiao, and Q. Luo, Hybrid density functional study of bandgaps for 27 new proposed half-Heusler semiconductors, *Journal of Applied Physics* **122**, 215701 (2017).
- [86] D. I. Bilc and P. Ghosez, Electronic and thermoelectric properties of Fe_2VAI : the role of defects and disorder, *Physical Review B* **83**, 205204 (2011).
- [87] S. Jana, A. Patra, and P. Samal, Assessing the performance of the Tao-Mo semilocal density functional in the projector-augmented-wave method, *The Journal of Chemical Physics* **149**, 044120 (2018).
- [88] J. Paier, M. Marsman, K. Hummer, G. Kresse, I. C. Gerber, and J. G. Ángyán, Screened hybrid density functionals applied to solids, *The Journal of Chemical Physics* **124**, 154709 (2006).
- [89] Y. Fu and D. J. Singh, Density functional methods for the magnetism of transition metals: SCAN in relation to other functionals, *Phys. Rev. B* **100**, 045126 (2019).
- [90] P. Janthon, S. A. Luo, S. M. Kozlov, F. Viñes, J. Limtrakul, D. G. Truhlar, and F. Illas, Bulk properties of transition metals: A challenge for the design of universal density functionals, *Journal of Chemical Theory and Computation* **10**, 3832 (2014).
- [91] M. Zahedifar and P. Kratzer, Band structure and thermoelectric properties of half-Heusler semiconductors from many-body perturbation theory, *Physical Review B* **97**, 035204 (2018).
- [92] W. Gao, T. A. Abtew, T. Cai, Y.-Y. Sun, S. Zhang, and P. Zhang, On the applicability of hybrid functionals for predicting fundamental properties of metals, *Solid State Communications* **234**, 10 (2016).
- [93] J. E. Coulter, E. Manousakis, and A. Gali, Limitations of the hybrid functional approach to electronic structure of transition metal oxides, *Physical Review B* **88**, 041107 (2013).
- [94] D. Golze, M. Dvorak, and P. Rinke, The GW compendium: A practical guide to theoretical photoemission spectroscopy, *Frontiers in Chemistry* **7**, 377 (2019).
- [95] S. Acharya, D. Pashov, A. N. Rudenko, M. Rösner, M. van Schilfgaarde, and M. I. Katsnelson, Importance of charge self-consistency in first-principles description of strongly correlated systems, *npj Computational Materials* **7**, 208 (2021).
- [96] H. Jiang, First-principles approaches for strongly correlated materials: A theoretical chemistry perspective, *International Journal of Quantum Chemistry* **115**, 722 (2015).
- [97] A. Yamasaki and T. Fujiwara, Electronic structure of transition metals Fe, Ni and Cu in the GW approximation, *Journal of the Physical Society of Japan* **72**, 607 (2003).
- [98] T. Kotani and M. van Schilfgaarde, Spin wave dispersion based on the quasiparticle self-consistent GW method: NiO, MnO and α -MnAs, *Journal of Physics: Condensed Matter* **20**, 295214 (2008).
- [99] E. Gürbüz, M. Tas, E. Şaşıoğlu, I. Mertig, B. Sanyal, and I. Galanakis, First-principles prediction of energy bandgaps in 18-valence electron semiconducting half-Heusler compounds: Exploring the role of exchange and correlation, *Journal of Applied Physics* **134**, 205703 (2023).
- [100] M. Tas, E. Şaşıoğlu, C. Friedrich, and I. Galanakis, A first-principles DFT+GW study of spin-filter and spin-gapless semiconducting Heusler compounds, *Journal of magnetism and magnetic materials* **441**, 333 (2017).
- [101] S. V. Faleev, M. Van Schilfgaarde, and T. Kotani, All-electron self-consistent GW approximation: Application to Si, MnO, and NiO, *Physical Review Letters* **93**, 126406 (2004).
- [102] M. van Schilfgaarde, T. Kotani, and S. Faleev, Quasiparticle Self-Consistent GW Theory, *Phys. Rev. Lett.* **96**, 226402 (2006).
- [103] M. Shishkin, M. Marsman, and G. Kresse, Accurate quasiparticle spectra from self-consistent GW calculations with vertex corrections, *Physical Review Letters* **99**, 246403 (2007).
- [104] B. Cunningham, M. Grüning, D. Pashov, and M. Van Schilfgaarde, QSGW: Quasiparticle self-consistent GW with ladder diagrams in W , *Physical Review B* **108**, 165104 (2023).
- [105] T. Kotani and H. Kino, Re-examination of half-metallic ferromagnetism for doped LaMnO_3 in a quasiparticle self-consistent GW method, *Journal of Physics: Condensed Matter* **21**, 266002 (2009).
- [106] T. Kotani, M. van Schilfgaarde, S. V. Faleev, and A. Chantis, Quasiparticle self-consistent GW method: a short summary, *Journal of Physics: Condensed Matter* **19**, 365236 (2007).
- [107] C. Friedrich, S. Blügel, and D. Nabok, Quasiparticle self-consistent GW study of simple metals, *Nanomaterials* **12**, 3660 (2022).
- [108] S. Ismail-Beigi, Justifying quasiparticle self-consistent schemes via gradient optimization in Baym-Kadanoff theory, *Journal of Physics: Condensed Matter* **29**, 385501 (2017).
- [109] S. L. Dudarev, G. A. Botton, S. Y. Savrasov, C. Humphreys, and A. P. Sutton, Electron-energy-loss spectra and the structural stability of nickel oxide: An LSDA+U study, *Physical Review B* **57**, 1505 (1998).
- [110] B. Himmetoglu, A. Floris, S. De Gironcoli, and M. Cococcioni, Hubbard-corrected DFT energy functionals: The LDA+U description of correlated systems, *International Journal of Quantum Chemistry* **114**, 14 (2014).
- [111] F. Zhou, M. Cococcioni, C. A. Marianetti, D. Morgan, and G. Ceder, First-principles prediction of redox potentials in transition-metal compounds with LDA+U, *Phys. Rev. B* **70**, 235121 (2004).
- [112] F. Aryasetiawan, K. Karlsson, O. Jepsen, and U. Schönberger, Calculations of Hubbard U from first-principles, *Physical Review B* **74**, 125106 (2006).
- [113] N. J. Mosey, P. Liao, and E. A. Carter, Rotationally invariant ab initio evaluation of Coulomb and exchange parameters for DFT+U calculations, *J. Chem. Phys.* **129** (2008).
- [114] H. J. Kulik, M. Cococcioni, D. A. Scherlis, and N. Marzari, Density functional theory in transition-metal chemistry: A self-consistent Hubbard U approach, *Phys. Rev. Lett.* **97**, 103001 (2006).
- [115] H. Jiang, R. I. Gomez-Abal, P. Rinke, and M. Scheffler, First-principles modeling of localized d states with the $\text{GW}@\text{LDA}+U$ approach, *Phys. Rev. B* **82**, 045108 (2010).
- [116] M. Kick, K. Reuter, and H. Oberhofer, Intricacies of DFT+U, not only in a numeric atom centered orbital framework, *Journal of Chemical Theory and Computa-*

- tion **15**, 1705 (2019).
- [117] H. C. Kandpal, G. H. Fecher, and C. Felser, Calculated electronic and magnetic properties of the half-metallic, transition metal based Heusler compounds, *Journal of Physics D: Applied Physics* **40**, 1507 (2007).
- [118] S. Wurmehl, G. H. Fecher, H. C. Kandpal, V. Ksenofontov, C. Felser, H.-J. Lin, and J. Morais, Geometric, electronic, and magnetic structure of Co_2FeSi : Curie temperature and magnetic moment measurements and calculations, *Phys. Rev. B* **72**, 184434 (2005).
- [119] A. Nourmohammadi and M. Abolhasani, First-principle study of full heusler Co_2YSi using PBE0 hybrid functional, *Solid State Communications* **150**, 1501 (2010).
- [120] E. Şaşıoğlu, I. Galanakis, C. Friedrich, and S. Blügel, Ab initio calculation of the effective on-site Coulomb interaction parameters for half-metallic magnets, *Physical Review B* **88**, 134402 (2013).
- [121] G. H. Fecher and C. Felser, Substituting the main group element in cobalt-iron based Heusler alloys: $\text{Co}_2\text{FeAl}_{1-x}\text{Si}_x$, *Journal of Physics D: Applied Physics* **40**, 1582 (2007).
- [122] D. E. Mellah and K. Demmouche, Exchange-correlation and spin-orbit coupling effects in 18-electrons transparent conductors half-Heusler: Ab-initio study, *Computational Condensed Matter* **32**, e00690 (2022).
- [123] M. Baral, S. Banik, A. Chakrabarti, D. Phase, and T. Ganguli, Study of electronic structure of Co_2MnSn Heusler alloy by resonant photoemission spectroscopy and ab initio calculations, *Journal of Alloys and Compounds* **645**, 112 (2015).
- [124] E. Sasioglu, W. Beida, S. Ghosh, M. Tas, B. Sanyal, S. Lounis, S. Blügel, I. Mertig, and I. Galanakis, Itinerant versus localized magnetism in spin gapped metallic half-Heusler compounds: Stoner criterion and magnetic interactions, arXiv , 2506.03416 (2025).
- [125] M. Yu, S. Yang, C. Wu, and N. Marom, Machine learning the Hubbard U parameter in DFT+U using Bayesian optimization, *npj Computational Materials* **6**, 180 (2020).
- [126] S. Yang, D. Dardzinski, A. Hwang, D. I. Pikulin, G. W. Winkler, and N. Marom, First-principles feasibility assessment of a topological insulator at the InAs/GaSb interface, *Physical Review Materials* **5**, 084204 (2021).
- [127] M. Yu, S. Moayedpour, S. Yang, D. Dardzinski, C. Wu, V. S. Pribiag, and N. Marom, Dependence of the electronic structure of the EuS/InAs interface on the bonding configuration, *Physical Review Materials* **5**, 064606 (2021).
- [128] S. Yang, N. B. M. Schröter, V. N. Strocov, S. Schuwalow, M. Rajpalk, K. Ohtani, P. Krogstrup, G. W. Winkler, J. Gukelberger, D. Gresch, G. Aeppli, R. M. Lutchyn, and N. Marom, Electronic structure of inas and insb surfaces: Density functional theory and angle-resolved photoemission spectroscopy, *Advanced Quantum Technologies* **5**, 2100033 (2022).
- [129] M. J. A. Jardine, D. Dardzinski, M. Yu, A. Purkayastha, A.-H. Chen, Y.-H. Chang, A. Engel, V. N. Strocov, M. Hocevar, C. Palmstrøm, S. M. Frolov, and N. Marom, First-principles assessment of CdTe as a tunnel barrier at the α -Sn/InSb interface, *ACS Applied Materials & Interfaces* **15**, 16288 (2023).
- [130] M. J. Jardine, D. Dardzinski, Z. Cai, V. N. Strocov, M. Hocevar, C. J. Palmstrøm, S. M. Frolov, and N. Marom, First-principles assessment of ZnTe and CdSe as prospective tunnel barriers at the InAs/Al interface, *ACS Applied Materials & Interfaces* **17**, 5462 (2025).
- [131] J. P. Perdew, K. Burke, and M. Ernzerhof, Generalized gradient approximation made simple, *Phys. Rev. Lett.* **77**, 3865 (1996).
- [132] J. P. Perdew, K. Burke, and M. Ernzerhof, Generalized gradient approximation made simple [Phys. Rev. Lett. **77**, 3865 (1996)], *Phys. Rev. Lett.* **78**, 1396 (1997).
- [133] J. Heyd, G. E. Scuseria, and M. Ernzerhof, Hybrid functionals based on a screened Coulomb potential, *J. Chem. Phys.* **118**, 8207 (2003).
- [134] J. Heyd, G. E. Scuseria, and M. Ernzerhof, Erratum: “Hybrid functionals based on a screened Coulomb potential” [J. Chem. Phys. **118**, 8207 (2003)], *The Journal of Chemical Physics* **124**, 219906 (2006).
- [135] W. P. Huhn and V. Blum, One-hundred-three compound band-structure benchmark of post-self-consistent spin-orbit coupling treatments in density functional theory, *Phys. Rev. Materials* **1**, 033803 (2017).
- [136] G. Kresse and J. Hafner, Ab initio molecular dynamics for liquid metals, *Phys. Rev. B* **47**, 558 (1993).
- [137] G. Kresse and D. Joubert, From ultrasoft pseudopotentials to the projector augmented-wave method, *Phys. Rev. B* **59**, 1758 (1999).
- [138] P. E. Blöchl, Projector augmented-wave method, *Phys. Rev. B* **50**, 17953 (1994).
- [139] P. Mavropoulos, I. Galanakis, V. Popescu, and P. H. Dederichs, The influence of spin-orbit coupling on the band gap of Heusler alloys, *Journal of Physics: Condensed Matter* **16**, S5759 (2004).
- [140] M. Shishkin and G. Kresse, Self-consistent GW calculations for semiconductors and insulators, *Physical Review B* **75**, 235102 (2007).
- [141] G. Pizzi, V. Vitale, R. Arita, S. Blügel, F. Freimuth, G. Géranton, M. Gibertini, D. Gresch, C. Johnson, T. Koretsune, J. Ibañez-Azpiroz, H. Lee, J.-M. Lihm, D. Marchand, A. Marrazzo, Y. Mokrousov, J. I. Mustafa, Y. Nohara, Y. Nomura, L. Paulatto, S. Poncé, T. Ponweiser, J. Qiao, F. Thöle, S. S. Tsirkin, M. Wierzbowska, N. Marzari, D. Vanderbilt, I. Souza, A. A. Mostofi, and J. R. Yates, Wannier90 as a community code: new features and applications, *Journal of Physics: Condensed Matter* **32**, 165902 (2020).
- [142] D. Wegner, A. Bauer, Y. M. Koroteev, G. Bihlmayer, E. Chulkov, P. Echenique, and G. Kaindl, Surface electronic structures of La (0001) and Lu (0001), *Physical Review B* **73**, 115403 (2006).
- [143] D. Dardzinski, M. Yu, S. Moayedpour, and N. Marom, Best practices for first-principles simulations of epitaxial inorganic interfaces, *Journal of Physics: Condensed Matter* **34**, 233002 (2022).
- [144] S. Wurmehl, G. H. Fecher, and C. Felser, Co_2CrIn : a further magnetic heusler compound, *Zeitschrift für Naturforschung B* **61**, 749 (2006).
- [145] A. Wolter, A. Bosse, D. Baabe, I. Maksimov, D. Mienert, H. Klauß, F. Litterst, D. Niemeier, R. Michalak, C. Geibel, *et al.*, Structure and magnetic order of the Heusler compound Co_2NbSn , *Physical Review B* **66**, 174428 (2002).
- [146] M. Gotoh, M. Ohashi, T. Kanomata, and Y. Yamaguchi, Spin reorientation in the new Heusler alloys Ru_2MnSb and Ru_2MnGe , *Physica B: Condensed Matter* **213**, 306 (1995).

- [147] P. Webster, Magnetic and chemical order in Heusler alloys containing cobalt and manganese, *Journal of Physics and Chemistry of Solids* **32**, 1221 (1971).
- [148] P. J. Brown, K. U. Neumann, P. J. Webster, and K. R. A. Ziebeck, The magnetization distributions in some Heusler alloys proposed as half-metallic ferromagnets, *Journal of Physics: Condensed Matter* **12**, 1827 (2000).
- [149] H. Chandra Kandpal, V. Ksenofontov, M. Wojcik, R. Seshadri, and C. Felser, Electronic structure, magnetism and disorder in the heusler compound Co_2TiSn , *Journal of Physics D: Applied Physics* **40**, 1587 (2007).
- [150] L. Bainsla and K. Suresh, Spin polarization studies in half-metallic Co_2TiX ($X = \text{Ge}$ and Sn) Heusler alloys, *Current Applied Physics* **16**, 68 (2016).
- [151] J. Barth, G. H. Fecher, B. Balke, S. Ouardi, T. Graf, C. Felser, A. Shkabko, A. Weidenkaff, P. Klaer, H. J. Elmers, H. Yoshikawa, S. Ueda, and K. Kobayashi, Itinerant half-metallic ferromagnets Co_2TiZ ($Z = \text{Si}, \text{Ge}, \text{Sn}$): Ab initio calculations and measurement of the electronic structure and transport properties, *Phys. Rev. B* **81**, 064404 (2010).
- [152] R. Ooka, I. Shigeta, Y. Sukino, Y. Fujimoto, R. Y. Umetsu, Y. Miura, A. Nomura, K. Yubuta, T. Yamauchi, T. Kanomata, and M. Hiroi, Magnetization and Spin Polarization of Heusler Alloys Co_2TiSn and $\text{Co}_2\text{TiGa}_{0.5}\text{Sn}_{0.5}$, *IEEE Magnetics Letters* **8**, 3101604 (2017).
- [153] P. Webster and K. Ziebeck, Magnetic and chemical order in Heusler alloys containing cobalt and titanium, *Journal of Physics and Chemistry of Solids* **34**, 1647 (1973).
- [154] T. Kanomata, T. Sasaki, H. Nishihara, H. Yoshida, T. Kaneko, S. Hane, T. Goto, N. Takeishi, and S. Ishida, Magnetic properties of ferromagnetic Heusler alloy Co_2ZrAl , *Journal of Alloys and Compounds* **393**, 26 (2005).
- [155] K. Buschow and P. van Engen, Magnetic and magneto-optical properties of Heusler alloys based on aluminium and gallium, *Journal of Magnetism and Magnetic Materials* **25**, 90 (1981).
- [156] K. Ziebeck and P. Webster, A neutron diffraction and magnetization study of Heusler alloys containing Co and Zr, Hf, V or Nb, *Journal of Physics and Chemistry of Solids* **35**, 1 (1974).
- [157] T. Shinohara, Nuclear magnetic resonance in Heusler alloys: Ni_2MnSn , Co_2MnSn and Ni_2MnSb , *Journal of the Physical Society of Japan* **28**, 313 (1970).
- [158] K. Buschow, P. van Engen, and R. Jongebreur, Magneto-optical properties of metallic ferromagnetic materials, *Journal of Magnetism and Magnetic Materials* **38**, 1 (1983).
- [159] J. Paier, M. Marsman, and G. Kresse, Why does the B3LYP hybrid functional fail for metals?, *The Journal of Chemical Physics* **127**, 024103 (2007).
- [160] B. Varaprasad, A. Rajanikanth, Y. Takahashi, and K. Hono, Highly spin-polarized $\text{Co}_2\text{MnGa}_{0.5}\text{Sn}_{0.5}$ Heusler compound, *Acta Materialia* **57**, 2702 (2009).
- [161] R. J. Soulen, J. M. Byers, M. S. Osofsky, B. Nadgorny, T. Ambrose, S. F. Cheng, P. R. Broussard, C. T. Tanaka, J. Nowak, J. S. Moodera, A. Barry, and J. M. D. Coey, Measuring the spin polarization of a metal with a superconducting point contact, *science* **282**, 85 (1998).
- [162] B. Nadgorny, M. S. Osofsky, D. J. Singh, G. T. Woods, R. J. Soulen Jr, M. K. Lee, S.-D. Bu, and C.-B. Eom, Measurements of spin polarization of epitaxial SrRuO_3 thin films, *Applied Physics Letters* **82**, 427 (2003).
- [163] H. Zhang, T. Pincelli, C. Jozwiak, T. Kondo, R. Ernstorfer, T. Sato, and S. Zhou, Angle-resolved photoemission spectroscopy, *Nature Reviews Methods Primers* **2**, 54 (2022).
- [164] H. Iwasawa, T. Ueno, T. Iwata, K. Kuroda, K. A. Kokh, O. E. Tereshchenko, K. Miyamoto, A. Kimura, and T. Okuda, Efficiency improvement of spin-resolved ARPES experiments using Gaussian process regression, *Scientific Reports* **14**, 20970 (2024).
- [165] Y. Miura, M. Shirai, and K. Nagao, Ab initio study on stability of half-metallic Co-based full-Heusler alloys, *Journal of Applied Physics* **99** (2006).
- [166] S. C. Lee, T. D. Lee, P. Blaha, and K. Schwarz, Magnetic and half-metallic properties of the full-Heusler alloys Co_2TiX ($X = \text{Al}, \text{Ga}, \text{Si}, \text{Ge}, \text{Sn}, \text{Sb}$), *Journal of Applied Physics* **97**, 10C307 (2005).
- [167] M. C. Hickey, A. Husmann, S. N. Holmes, and G. A. C. Jones, Fermi surfaces and electronic structure of the Heusler alloy Co_2TiSn , *Journal of Physics: Condensed Matter* **18**, 2897 (2006).
- [168] B. Varaprasad, A. Srinivasan, Y. Takahashi, M. Hayashi, A. Rajanikanth, and K. Hono, Spin polarization and Gilbert damping of $\text{Co}_2\text{Fe}(\text{Ga}_x\text{Ge}_{1-x})$ Heusler alloys, *Acta Materialia* **60**, 6257 (2012).
- [169] P. Klaer, B. Balke, V. Alijani, J. Winterlik, G. Fecher, C. Felser, and H. Elmers, Element-specific magnetic moments and spin-resolved density of states in CoFeMnZ ($Z = \text{Al}, \text{Ga}, \text{Si}, \text{Ge}$), *Physical Review B* **84**, 144413 (2011).